Numerical Simulations of Stratus Clouds and Their Sensitivity to Radiation—A RACE Case Study

HONG GUAN, ANDRÉ TREMBLAY, AND GEORGE A. ISAAC

Cloud Physics Research Division, Meteorological Service of Canada, Downsview, Ontario, Canada

KEVIN B. STRAWBRIDGE

Air Quality Processes Research Division (CARE), Meteorological Service of Canada, Egbert, Ontario, Canada

CATHARINE M. BANIC

Cloud Physics Research Division, Meteorological Service of Canada, Downsview, Ontario, Canada

(Manuscript received 2 November 1998, in final form 16 January 2000)

ABSTRACT

The three-dimensional Canadian Mesoscale Compressible Community model has been run at high resolution ($\Delta x = 2$ km, $\Delta z = 50$ m) to simulate stratus clouds observed on 1 September 1995 during the Radiation, Aerosol and Cloud Experiment (RACE) conducted near the Bay of Fundy, Canada. A new explicit cloud scheme and the Canadian operational radiation scheme were validated at this resolution for the first time. The simulations show a reasonable agreement between the observed and modeled stratus cloud system. The cloud structure, position, cloud water content, temperature, and the qualitative properties of longwave and shortwave radiative fluxes were verified against the satellite imagery, lidar, and aircraft measurements taken during RACE. The simulated cloud thickness (~150 m) was thinner than the observed one (200–250 m). The differences in the simulated and observed radiative fluxes were mainly due to errors in the simulation of cloud thickness. Sensitivity experiments demonstrate that the simulated cloud is extremely sensitive to longwave and shortwave radiation. Longwave (shortwave) radiation substantially increased (decreased) the total water path.

1. Introduction

It is well known that stratocumulus and stratus cover about 34% of the oceans and 18% of land surface at any given time (Heymsfield 1993; Considine et al. 1997). These low-level clouds play an important role in the global energy budget. For this reason, much effort has been invested in studying this class of cloud through field campaigns [First ISCCP Regional Experiment (FIRE), Stratocumulus (Albrecht et al. 1988), Atlantic Stratocumulus Transition Experiment (ASTEX; Albrecht et al. 1995), Southern Ocean Cloud Experiment (SOCEX; Boers et al. 1996)] and through modeling studies (Chen and Cotton 1983; Nicholls 1984; Moeng 1986; Driedonks and Duynkerke 1989; Duynkerke 1989; Koracin and Rogers 1990; Moeng and Schumann 1991; Moeng et al. 1992; Rogers and Koracin 1992; Albrecht 1993; Kogan et al. 1995; Krueger et al. 1995a,b; Feingold et al. 1997).

The Mesoscale Compressible Community (MC2) model has been used successfully to study a wide spectrum of phenomenon ranging from microscale supersonic waves, through small-scale local convection, to large-scale synoptic weather systems. However, the ability of MC2 to simulate a stratiform cloud system had not been examined. The main goal of this paper is to demonstrate the ability of MC2 to simulate a stratiform cloud system at high resolution. A new cloud scheme (Tremblay et al. 1996) and radiation model will be assessed against satellite, lidar, and aircraft observations. The ways to further improve cloud and radiative property forecasts will be suggested. This is important because the new cloud scheme will replace the Sundqvist cloud scheme in future Canadian operational forecast model. The in situ aircraft observations were made during the Radiation, Aerosol and Cloud Experiment (RACE) held in August–September 1995 over the Bay of Fundy and Gulf of Maine. This provides an opportunity to make a direct comparison between model results and in situ aircraft data along the aircraft track.

Corresponding author address: Dr. Hong Guan, Meteorological Service of Canada, 4905 Dufferin Street ARMP, Downsview, ON M3H 5T4, Canada
E-mail: hong.guan@ec.gc.ca

The sensitivity of the simulated cloud on the longwave and shortwave radiation will also be examined and studied.

A single-layer stratus cloud case (1 September 1995) was selected for simulation and study. Airborne observations were made with both the National Research Council of Canada Twin Otter and the Convair-580 aircraft. Cloud water, air temperature, water vapor content, broadband longwave radiative fluxes (3.5–50 μm), and broadband shortwave radiative fluxes (0.3–2.8 μm) were measured. This dataset is suitable to test the numerical model, cloud, and radiation schemes.

The Convair-580 carried a dual-wavelength (1064 nm at 5.0 mrad and 532 nm at 0.9 mrad) 10 Hz Nd:YAG lidar system operating in a near-nadir orientation (Strawbridge and Li 1997). For the current case, we use 1-s averaged lidar data with a vertical resolution of 12 m made from an altitude of 3 km above sea level to obtain cloud structure and reflectivity. The Twin Otter obtained simultaneous in situ measurements below.

The paper is organized as follows. The following section describes the MC2 model, the explicit cloud scheme and the radiation code. In section 3, the meteorological conditions for the case under study (1 September 1995) are described. In section 4, the simulation results are presented and compared with the satellite, lidar, and aircraft observations. Section 5 examines the sensitivity of the simulated cloud on the longwave and shortwave radiation, and the conclusions are summarized in section 6.

2. Model description and numerical experiment design

The MC2 model is based on fully compressible, nonhydrostatic Euler equations, and a complete description of the model can be found in Tanguay et al. (1990), Bergeron et al. (1994), and Desgagne et al. (1995). The fundamental features of the model include variable vertical resolution, a complete set of physical processes, time-dependent nesting of the lateral boundary conditions supplied by a larger-scale model, and a modified Gal-Chen terrain-following vertical coordinate. The model was successfully applied to various scale simulations (Robert 1993; Tremblay 1994; Tremblay et al. 1996; Kong and Yau 1997; Szeto et al. 1999).

a. Radiative transfer model

The broad-band longwave (infrared) radiation model of Garand (Garand 1983; Garand and Mailhot 1990) is used to compute the longwave radiative fluxes and cooling rate in the cloud and atmosphere. The model takes into account the radiative effects of water vapor, carbon dioxide, ozone, and clouds with tabulated transmission functions based on the high-resolution transmission molecular absorption (Rothman et al. 1987) spectroscopic databank. Clouds are assumed to be gray and nonscattering. The multiplication approximation is used to take into account the effect of overlapping among different gas and cloud absorptions.

The shortwave (visible) radiation model is based on the Fouquart and Bonnel's (1980) scheme. The scheme calculates the shortwave radiative fluxes and solar heating rate in the cloud and atmosphere. The scheme takes into account the effects of water vapor, carbon dioxide, ozone, and clouds, and considers Raleigh diffusion and multiple scattering. Three basic shortwave cloud optical parameters (the asymmetry factor, the single-scattering albedo, and the optical depth) were parameterized following Slingo (1989). All parameters are related to the effective droplet radius (r_e) defined as the ratio of the third to second moment of the cloud drop size distribution, while the optical depth is also related to cloud water path. The effective radius of cloud droplets is parameterized assuming a Gamma distribution (Barker 1992) verified to be realistic from aircraft measurements of water droplet spectra

$$r_e = 754.6\left(\frac{\mathrm{LWC}d_a}{N}\right)^{1/3}, \tag{1}$$

with r_e in micrometers, d_a the air density (kg m^{-3}), and N the number of cloud drops per cubic centimeter taken as 100 over oceans and 500 over land. In the original shortwave radiation code (Canadian operational code), the optical depth is reduced to 30% of the value proposed by the parameterization to take into account inhomogeneities in the distribution of cloud water in a model grid box and to compensate for the assumption of a plane-parallel atmosphere as revealed by Barker (1992) and Cahalan et al. (1995). The global shortwave budget matches the available climatology after the above adjustment (Yu et al. 1997). A slightly different adjustment factor (40%) was used in the current work since the effect of cloud inhomogeniety is smaller in a higher resolution model.

For the high-resolution runs (10 km, 2 km) in the current study, the model-predicted grid-scale ice–liquid water contents are directly coupled into the radiation model, which provides full cloud–radiation interactions.

b. Cloud schemes

To compare the simulation results with aircraft observations, high-resolution simulations are needed. For the high-resolution runs, a horizontal resolution of 2 km and a vertical resolution of 50 m within the lowest 1.3 km are employed. This leads to a small time step (30 s) for numerical stability. The high-resolution grid and small time step consume a large amount of central processing unit time. Therefore, a fast and efficient cloud scheme is required for our study. The new mixed-phase cloud scheme developed by Tremblay et al. (1996) is used to produce solid and liquid phase water. The scheme only involves a single prognostic equation for total water content. However, when the temperature is

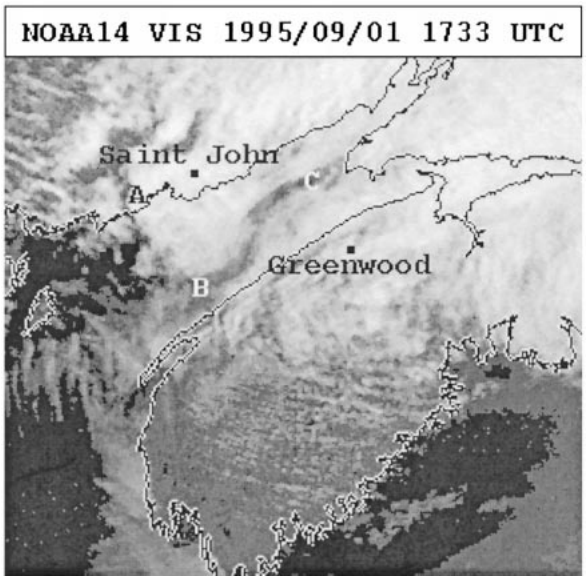

FIG. 1. NOAA visible image for 1733 UTC 1 Sep 1995. The locations of the boundary between the cloud and clear regions over the Bay are denoted along AB and BC, respectively.

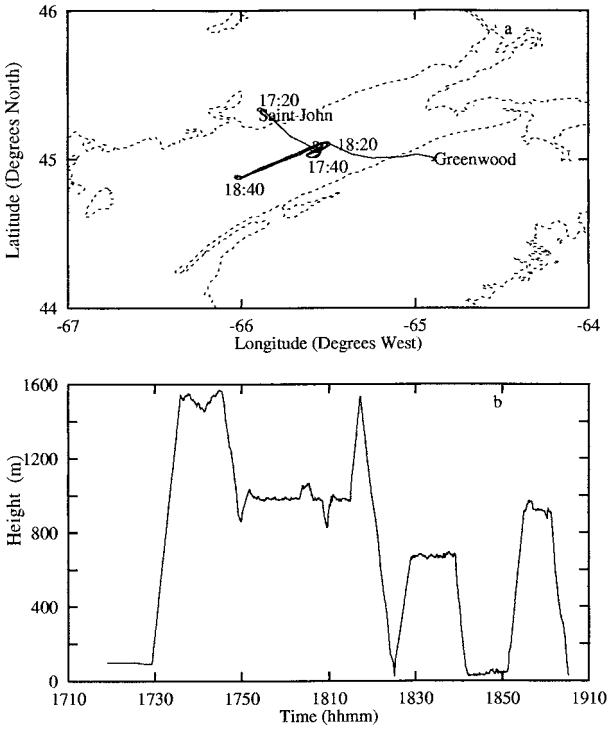

FIG. 2. (a) Horizontal projection of aircraft trajectory for the flight 13c. (b) Height along aircraft trajectory for the flight 13c. The time period for which the research aircraft sampled along a northeast–southwest line is between 1740 and 1850 UTC.

below 0°C, the total water content is partitioned diagnostically into solid and liquid phases. A detailed description of the scheme can be found in Tremblay et al. (1996).

c. Numerical simulation setup

A 36-h integration at 50-km resolution during the period from 1200 UTC 31 August to 0000 UTC 2 September 1995, was generated. Canadian Meteorological Center (CMC) analysis data were used to initialize the model. At the time of the RACE, the CMC analysis system routinely produced wind components, dewpoint depression, temperature, geopotential height fields at 15 standard pressure levels (from 10 to 1000 mb). To initialize the Recherche en Prévision Numérique (RPN) physics package, a set of mutually consistent ''geophysical'' parameters is required. Time-invariant quantities currently include mean terrain height, launching height, land–sea mask, and roughness length for the turbulent surface fluxes. Time-dependent quantities, either from monthly climatology or gridded from the observations valid at initial time, are surface temperature, deep soil temperature, soil wetness, snow fraction on ground, sea ice, and surface albedo. The Kuo cumulus parameterization (Kuo 1974) and Sundqvist resolved-scale condensation technique (Sundqvist et al. 1989) were used.

To compare the simulation results with the aircraft observations, a series of nested runs with the mixed-phase cloud scheme were carried out with a horizontal resolution of 25, 10, and 2 km. For the nested simulations, the result from the coarser-resolution run was used to provide initial and boundary conditions for the finer one. The Fritsch–Chappell convective parameterization scheme (Fritsch and Chappell 1980; Zhang and Fritsch 1986) was utilized in the 25-km run. No convective parameterization scheme was selected for the cloud-scale simulations (10 km, 2 km). In this investigation, we will mainly focus on the results for a horizontal resolution of 2 km to allow comparison with the aircraft and lidar observations.

For the simulations with a horizontal resolution of 2 km, the domain is 300 km $\times$ 300 km. With 53 vertical Gal-Chen levels and a 25 km model lid, the smallest vertical grid size is 50 m within the lowest 1.3 km and the largest grid size is about 2500 m near the top of the domain. The flight track was approximately located in the center of the domain.

3. Flight 13c case and aircraft data

The visible satellite image in Fig. 1 shows the stratiform cloud system near the Bay of Fundy at 1733 UTC 1 September 1995. It can be seen that the cloud extends from the northeast to the southwest over the bay. The boundary between cloudy and clear regions over the bay can be noted along AB. The horizontally inhomogeneous structure of the cloud over the bay is also evident in this image. Most obvious is the existence of a clear region along BC. The cloud seems thicker in the

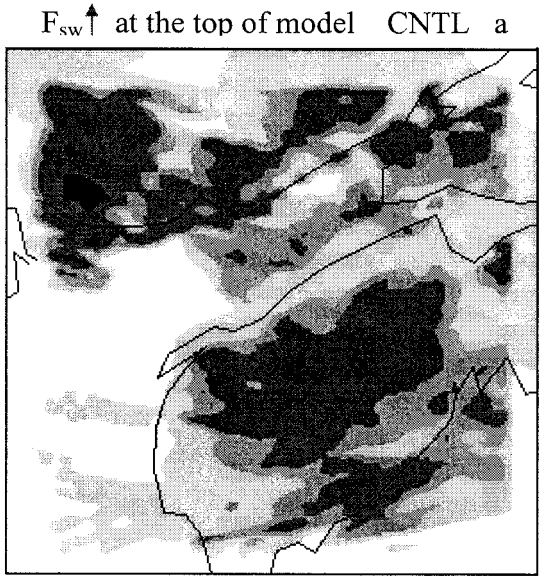

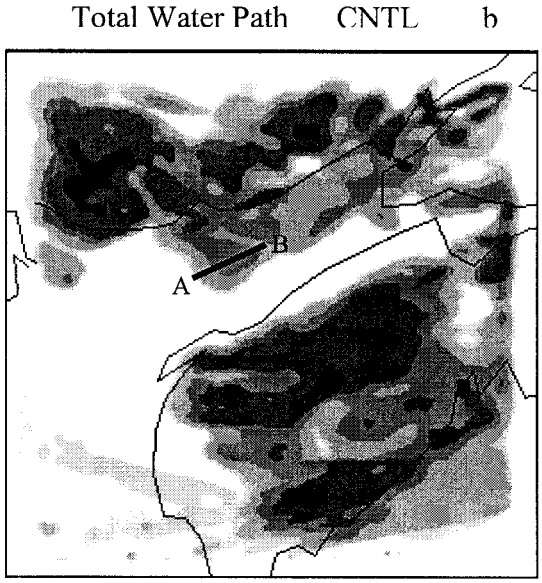

FIG. 3. (a) Upward shortwave radiative flux at the top level of model at 1800 UTC 1 Sep 1995. The stippled areas from light to dark represent 150, 250, 300, 400 W m^{-2}, respectively. (b) Total water path at 1800 UTC 1 Sep 1995. The stippled areas from light to dark represent 0.005, 0.01, 0.03, 0.05, 0.1 mm, respectively.

area close to Saint John, New Brunswick (NB) than that in the rest of the bay.

Figure 2a gives a horizontal projection of the Twin Otter research aircraft trajectory. The aircraft took off from Saint John, and flew southeast to arrive at the center of the bay. Then, it continuously sampled along a northeast–southwest line. The cloud boundary was encountered at the southwest side of the aircraft track. Last, the aircraft landed at Greenwood, Nova Scotia.

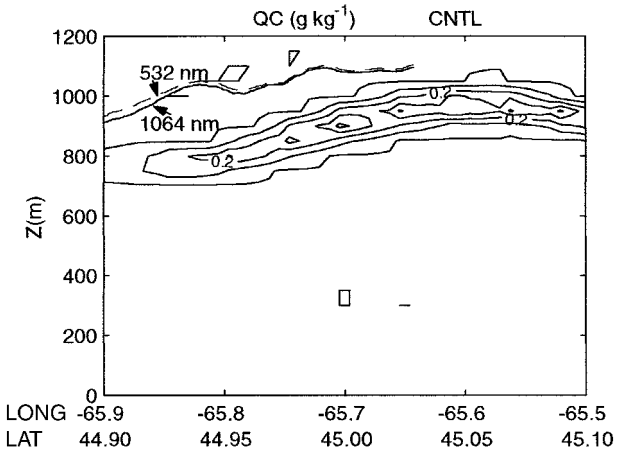

FIG. 4. Vertical cross section of cloud water content along line AB of Fig. 3b at 1800 UTC 1 Sep 1995 for the CNTL run. Cloud-top heights derived from the lidar reflectivity obtained from 1745 to 1758 UTC are indicated by the solid (1064 nm) and dashed (532 nm) lines.

The time series of aircraft altitude is displayed in Fig. 2b. It can be noted that the aircraft climbed to an altitude of 1500 m (above cloud top), then descended to a lower level to obtain some information above, within and below the cloud. The flight record indicates that a single-layer stratus cloud prevailed during this flight. The aircraft data provides a quantitative sampling of the stratiform cloud system and information about cloud base, top, and thickness.

During the Twin Otter flight, the Convair with the downward-looking lidar sampled above the cloud along a similar track as the Twin Otter.

4. Case simulations

In this section, the control simulation (CNTL) is verified against satellite, lidar, and aircraft observations.

Figures 3a,b depict the upward shortwave radiative flux at the top level of the domain and the vertically integrated total water (total water path) at 1800 UTC 1 September 1995. In general, the pattern of the simulated upward shortwave radiative flux is in reasonable agreement with the satellite imagery over the Bay of Fundy (see Fig. 1). The boundary between the cloud and clear regions is well simulated. The inhomogenous feature of the cloud over the Bay of Fundy is also very similar to the observed one (i.e., a clear region over the bay, and the cloud is thicker in the region close to Saint John, NB than over the rest of the bay). The correlation between the upward shortwave radiative flux (Fig. 3a) and the total water path pattern (Fig. 3b) is apparent. The strong upward shortwave radiative flux is associated with the larger total water path, thus, larger optical thickness. The total water path over the bay is very small (maximum value is between 0.04 and 0.05 mm). However, the value over the land (maximum is more than 0.1 mm) is much larger than that over the bay.

To verify the simulated cloud top, Fig. 4 displays the vertical cross section of the simulated cloud water content at 1800 UTC 1 September 1995 and the cloud-top height derived from the lidar reflectivity between 1745 and 1758 UTC 1 September 1995 along the line AB of Fig. 3b. A cloud-top algorithm was developed to obtain cloud-top heights from both the 1064 nm and 532 nm lidar data. Cloud top is determined from the lidar profile data by calculating the height at which the first derivative of the lidar backscatter becomes a maximum. The error in cloud-top height is 24 m: the combined error of the detection algorithm of both the cloud and surface assuming the aircraft altitude was constant along this short flight track. The difference in cloud top derived from the lidar reflectivity with the wavelength of 532 nm and 1064 nm is small. It can be noted that the simulated cloud top (between 800 m and 1050 m) changes with the horizontal position. The observed top also indicates the same change with the top between 925 m and 1100 m. Therefore, the simulated cloud top is lower than the lidar observed top. Based on Fig. 4, the simulated maximum cloud water content is located at the middle of the cloud, inconsistent with the observed, which indicates the maximum value is near the cloud top. This deficiency could be from the use of a poor vertical resolution (50 m), hardly adequate to resolve the fine vertical structure of a 200 m deep cloud layer.

To compare the simulated cloud and radiation features with the aircraft measurements, fields of temperature, cloud water content, downward (upward) shortwave radiative flux, and downward (upward) longwave radiative flux at 1800 UTC 1 September 1995 were interpolated in space along the aircraft flight path displayed in Fig. 2. The fields were also interpolated in both space and time along the flight path, which yields very similar results, indicating little change in the stratus system within 1 h and 45 min. These series were compared directly with aircraft measurements (Fig. 5). The aircraft data were averaged over the interval of 33 s, approximately 2-km flight paths, which were roughly comparable with the resolution of the model. The cloud base and top derived from aircraft altitude and liquid water content are also shown in Fig. 5.

Both the model and observations show four cloud tops and four cloud bases along the aircraft trajectory (Fig. 5a). As expected, the simulated cloud tops and bases are closer to the observed when the flight time is near the verification time of 1800 UTC. The observed cloud tops are 1080, 1120, and 1110 m near the verification time (from 1740 UTC to 1820 UTC). Thus, the average cloud top is 1100 m, which is about 100 m higher than the simulated cloud top (1000, 1000, 1000 m). The simulated cloud base (850 m) is only 30 m lower than the observed (880 m) at 1821 UTC. This leads to a thinner cloud (150 m) in the model than for the observation (220 m).

The simulated temperature compares well with the observed temperature during the aircraft measurements. The average difference between the two curves is about 0.78°C, close to the instrument error (±0.5°C). Some small-scale oscillations are successfully predicted. In particular, two locally low temperature signals marked with A and B are predicted, as the aircraft descended from a altitude of about 1500 m to the ground surface. The corresponding signals are also detected by the aircraft during that period. The signal A and B are, respectively, associated with the net cooling in the cloud and the temperature inversion near the cold ocean surface. The high correlation indicates the accuracy of MC2 in the high-resolution simulation.

The simulated and observed cloud water content along the aircraft track are compared in Fig. 5c. To facilitate data visualization, the cloud water measured aboard the aircraft has been multiplied by -1. In general, the model successfully produces observed cloud water content value (between 0.2 and 0.4 g kg^{-1}) except at the beginning of the flight, where the simulated value (0.2 g kg^{-1}) is significantly less than the observed (0.8 g kg^{-1}). A potential reason is the coarse vertical resolution (100 m) at elevated altitudes.

The tendency of the downward shortwave radiative flux (Fig. 5d) is reasonably simulated. This indicates that the model successfully predicted the existence and position of the stratus cloud. In the clear regions above the cloud top (marked with A and B), the simulated values are very close to the observed. The downward shortwave radiative flux is very sensitive to the cloud thickness above the flight level. For example, the observed and simulated downward shortwave radiative flux decreases by 525 and 375 W m^{-2}, respectively, as the aircraft flew down from the cloud top to the cloud base around 1820 UTC. The smaller change of downward shortwave radiative flux in the simulation is mainly due to the fact that the simulated cloud is thinner than the observed one. Because liquid water path (LWP) increases roughly as the square of cloud depth, the LWP in a cloud that is 150 m deep is less than half the LWP in a cloud that is 220 m deep. This large difference in LWP explains the large differences in the shortwave radiation signatures in the clouds.

The two upward shortwave radiative flux curves follow each other (Fig. 5e). The value is very small (less than 100 W m^{-2}) when the aircraft is under the cloud (marked with C and D), mainly due to the smaller downward shortwave radiative flux under the cloud and low surface albedo. As a result of the thinner cloud, the simulated upward shortwave radiative flux above the cloud top (marked with A and B) is lower than the observed.

The simulated tendency of the downward longwave radiative flux (Fig. 5f) during the flight is also in good agreement with the observation. A lower value indicates less cloud water path above the aircraft. Both the observations and simulation indicate a lower downward flux as the aircraft flew above the cloud top (marked with A and B). But, in general, the simulated value in

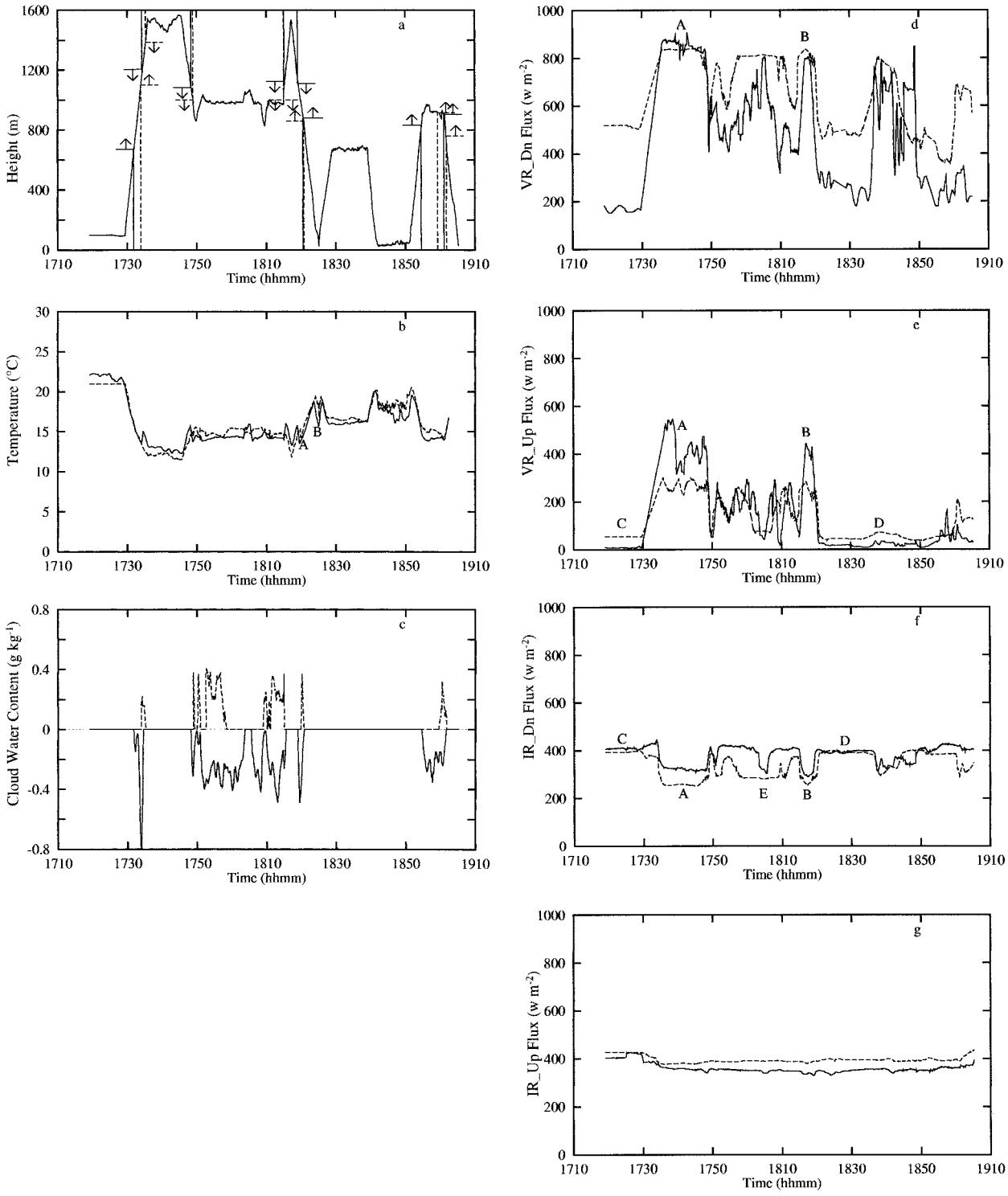

FIG. 5. (a) Simulated (dashed) and observed (solid) cloud top and base. A vertical line from above (below) to the aircraft altitude curve indicates cloud top (base). Simulated (dashed) and observed (solid) (b) temperature, (c) cloud water content (the cloud water measured aboard the aircraft has been multiplied by −1), (d) downward shortwave radiative flux, (e) upward shortwave radiative flux, (f) downward longwave radiative flux, and (g) upward longwave radiative flux along aircraft trajectory for the flight 13c.

the clear region is about 30–50 W m^{-2} lower than the Twin Otter's observation. This could be due to the inaccuracy of the simulated atmospheric profiles above the cloud top. A comparison of the longwave radiative flux data between the Twin Otter and Convair shows that the downward longwave radiative flux obtained from the Twin Otter is higher than the Convair value by 42 W m^{-2}, when both aircraft were under the same clear atmosphere and at the same height. Therefore, the difference between the simulation and observation may be partly induced by instrument error. Below the cloud (marked with C and D), the two curves are very close. The downward longwave radiative flux is mainly due to emission from the cloud base, where the simulated and observed temperatures are very similar. The large difference between 1757 and 1810 UTC (marked with E) is mainly because the simulated cloud top is lower than the observed, thus, a smaller downward longwave radiative flux from the clear atmosphere above the simulated cloud top is predicted by the model. A larger downward shortwave radiative flux and a smaller downward longwave radiative flux around 1840 UTC for both the curves verify that the cloud boundary at the southwest side of the aircraft track (see Fig. 2a) is successfully reproduced by the model.

Unlike the downward longwave radiative flux, the upward longwave radiative flux (Fig. 5g) is not sensitive to the existence of the cloud. For both cases, the curves are very flat. The upward longwave radiative flux is mainly due to the emissions from the ocean surface and cloud. The small temperature differences (2°–3°C for both observation and simulation) between the ocean surface and cloud lead to the flat curves. The average upward longwave radiative flux from the simulation is about 30 W m^{-2} higher than the observation. The error results from the following two factors. First, in the longwave radiation scheme, the emissivity from both the land and ocean is assumed to be 1. In fact, the ground surface is not exactly a blackbody. The emissivity from the ocean is about 0.94. The difference of 0.06 in emissivity could produce an error of about 20 W m^{-2} in the upward longwave radiative flux over the ocean. Second, the difference between the simulated and observed temperatures at the ocean surface is about 1°–2°C (the simulated value is higher), corresponding to about an error of 5–10 W m^{-2} in the upward longwave radiative flux. Because the longwave radiation model used in this study is the CMC operational model, the current ocean emissivity of 1 in the CMC model should be changed to more reasonable ocean emissivity (0.94), which may improve the upward longwave radiative flux, the longwave radiative heating rate at the cloud base, and forecasts of the cloud field.

The verification of the high-resolution simulation (CNTL simulation) shows that MC2 did indeed simulate the observed stratus system with a fair degree of accuracy. The horizontal and vertical positionings of the stratus cloud were close to the observed locations. The single-layer structure of the cloud was captured in the simulation. The simulated cloud water content was in reasonable accord with that observed by the research aircraft. The simulated and observed temperatures were highly correlated. The patterns of the shortwave and longwave radiative fluxes along the aircraft track were also comparable with the observations.

The simulated cloud-top height and thickness were underestimated, which leads to the differences in the radiative fluxes. Previous (Guan et al. 1997) and current studies (discussed in section 5) indicate that the distribution of cloud water is strongly affected by the feedback processes between radiation and clouds. Therefore, the underestimation of cloud thickness and top could originate from deficiencies of the shortwave radiation scheme. First, in the current radiation model, the cloud droplet spectrum was assumed to be a Gamma distribution with the N taken as 100 cm^{-3} over the ocean, while the aircraft observed N as 300 cm^{-3} for this case. Because the cloud optical depth is inversely proportional to N, the use of a smaller N in the model would induce a smaller optical depth and larger downward shortwave radiative flux below the cloud. Therefore, in order to obtain accurate cloud albedo and shortwave radiative fluxes, the cloud microphysical parameters should be predicted realistically by cloud models. Also, in the solar radiation model, the optical depth is reduced to 40% of the value proposed by the parameterization. However, this reduction factor varies with local time and presumably with season and region (Cahalan et al. 1994). The accuracy of this parameter should be further estimated once the correct cloud microphysics parameters are produced by a more sophisticated cloud model, which can explicitly predict the cloud droplet spectrum.

5. Sensitivity test

In this section, we will investigate the effects of shortwave and longwave radiation on the stratus cloud. In the first simulation, the shortwave absorption and scattering by condensate (NOSW) were turned off. In the second simulation, the longwave absorption and emission by condensate (NOLW) were excluded. For these two sensitivity tests, the radiative cooling and heating of the air and ground were still retained, only the effects of the cloud on radiative fluxes were set to zero.

The comparison between the CNTL and NOSW runs will give information about the effects of shortwave radiation on the stratus cloud. The importance of longwave radiation on the cloud maintenance and development will be found through a comparison of the NOLW simulation to the CNTL simulation.

a. Shortwave effects on cloud

To examine the total effect of shortwave radiation, the total water path at 1800 UTC 1 September 1995 for the NOSW run (Fig. 6) is compared with the CNTL run

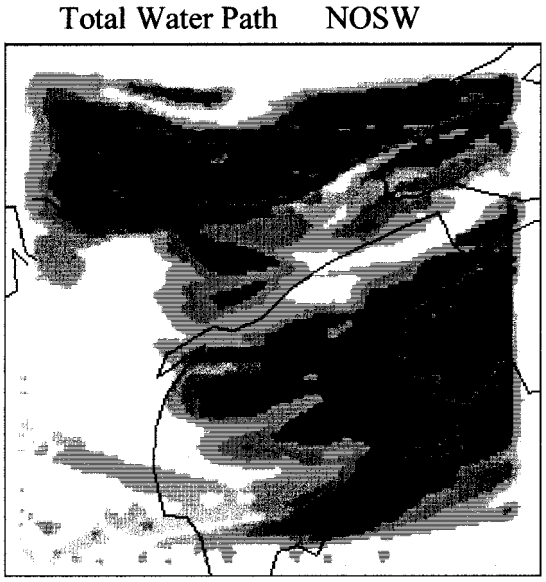

FIG. 6. Total water path at 1800 UTC 1 Sep 1995. The stippled areas from light to dark represent 0.005, 0.01, 0.05, 0.1, 0.3 mm, respectively.

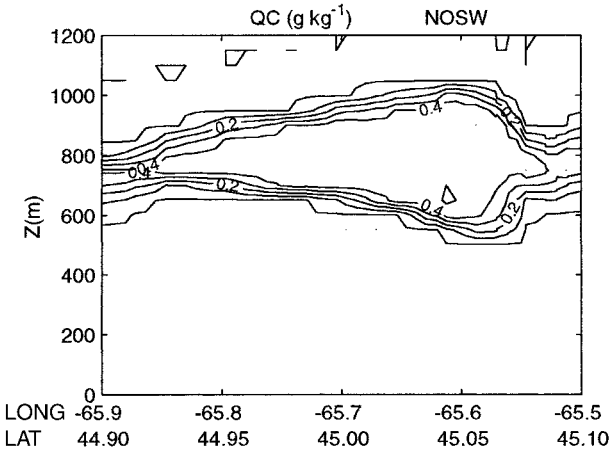

FIG. 7. Vertical cross section of cloud water content along line AB of Fig. 3b at 1800 UTC 1 Sep 1995 for the NOSW run.

(Fig. 3b). The horizontal distribution of the total water path for the both simulations is, in general, similar. The total water path is larger over the land than over the bay. However, the value is approximately 3–6 times larger in the NOSW run than that in the CNTL simulation. The stratus cloud over the bay covers a larger area in the NOSW case. The boundary between the cloud and the clear region further extends outward from the bay. Therefore, the shortwave radiation significantly damped the cloud development.

Figure 7 depicts the vertical cross section of the cloud water content along the line AB (see Fig. 3b) for the NOSW run at the same simulation time as Fig. 6. Figure 7 should be compared with the CTRL cross section of Fig. 4. By removing the effect of shortwave radiation, a thicker cloud with higher values of liquid water content was produced. The maximum cloud thickness is 400 m, which is about twice that in the CNTL. The cloud base is much lower, while the cloud top does not exhibit an important change (the cloud top is lower only within a small part near the longitude of $-65.55°$). For most of the cloud, the cloud water content is more than 0.4 g kg^{-1} (the maximum value is about 0.5 g kg^{-1}) in the NOSW, while the CNTL run shows a maximum value less than 0.4 g kg^{-1}.

Figure 8a shows the vertical cross section of shortwave radiative heating rates along the line AB for the CNTL simulation. It can be seen that there is shortwave heating throughout the entire cloud layer. The peak-heating rate is about 2.3 K h^{-1}. The heating rate in the clear atmosphere is less than 0.5 K h^{-1}. Turning off the shortwave radiation leads to a change in temperature field. Figure 9b exhibits the vertical cross sections of temperature difference (DT) between the NOSW and

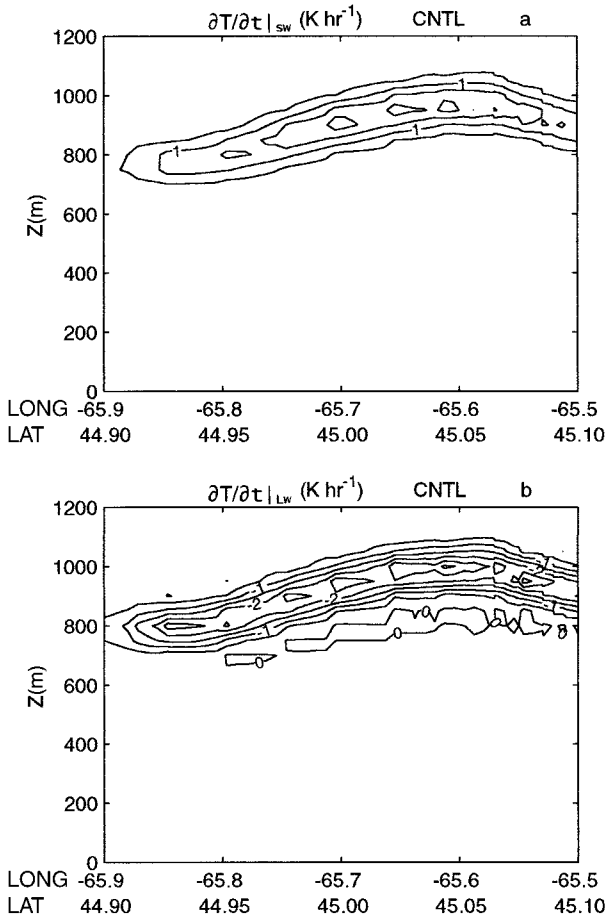

FIG. 8. Vertical cross section of (a) shortwave radiative heating and (b) longwave radiative cooling rates along the line AB of Fig. 3b at 1800 UTC 1 Sep 1995 for the CNTL run.

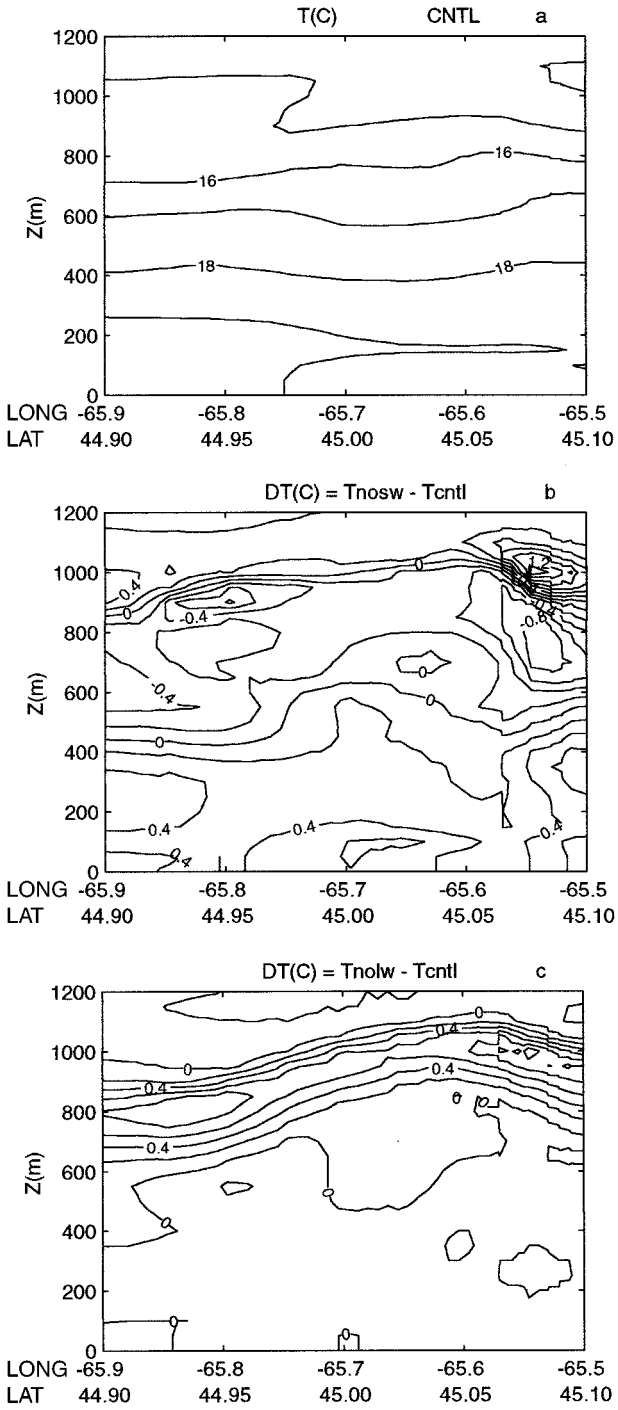

FIG. 9. Vertical cross section of (a) temperature for the CNTL run, (b) temperature difference between the NOSW and CNTL runs, and (c) temperature difference between the NOLW and CNTL runs along the line AB of Fig. 3b at 1800 UTC 1 Sep 1995.

CNTL experiments. Positive (negative) DT values denote regions where the temperature in the NOSW is warmer (colder) than the CNTL. When the effect on the cloud was set to zero, the model produced a cooler cloud and a warmer atmosphere below the cloud base. In the NOSW run, the ground surface and low-level atmosphere below the cloud obtained more shortwave energy, thereby, more heating. The maximum difference in the low-level atmosphere below the cloud base is 0.7°C (long = −65.52°, Z = 350 m). The maximum difference in the cloud is −0.96°C (long = −65.83°, Z = 900 m). A combination of cloud cooling and low-level atmospheric warming below the cloud results in a steeper temperature lapse rate below the cloud top and, consequently, a more unstable atmosphere for NOSW. The averaged temperature lapse rate below 850 m within the selected cross-section is about 6.5 K km^{-1}, 1 K km^{-1} larger than in the CNTL case. The difference in the cloud top between the NOSW and CNTL cases (See Fig. 4 and Fig. 7) causes a positive DT region (long = −65.56, Z = 1000 m). The cloud is colder in the CNTL than the clear atmosphere in the NOSW.

Figures 10a,b present the distributions of the vertically averaged turbulent kinetic energy between the ground surface and 1200 m, and the horizontal velocity vectors at a height of 900 m for the CNTL simulation. Before doing a comparison between the two simulations, the mechanism of cloud breakup over the bay will first be examined by using the results in the CNTL run. Vertically averaged turbulent kinetic energy is zero over the Bay of Fundy. In contrast, strong turbulent kinetic energy is prevalent over the land, particularly over New Brunswick. The values are between 0.5 and 1.5 m^2 s^{-2} over New Brunswick. This indicates that the moisture and heat can be effectively transported upward over the land because vertical diffusion coefficient is proportional to TKE$^{1/2}$ in the current model. Therefore, a larger total water path (Fig. 3b) over the land was formed through the stronger upward transfer of moisture and heat. Figure 10b shows that the wind blows from the northwest to the southeast over the bay. Therefore, the cloud over the bay is possibly advected from the land (New Brunswick). This fact is also verified by observing the time evolution of the satellite images (not shown). When the cloud moved from the land to the bay, the upward transport of heat and moisture was cut off. The stratus cloud became thinner. Last, a clear region appeared before it moved into Nova Scotia.

The patterns of the averaged turbulent kinetic energy are very similar for the CNTL and NOSW simulations (compare Fig. 11 with Fig. 10a). However, the values in the NOSW experiment are much larger than those in the CNTL case over the land. The values range from 1.5 to 2.5 m^2 s^{-2}. The larger turbulent kinetic energy leads to a larger total water path because of the stronger heat and moisture fluxes, which is consistent with Duynkerke's results in a one-dimensional simulation (1989). It can be noted that a small nonzero turbulent kinetic energy area occurs over the bay in the NOSW case, which is a result of the increase of the temperature lapse rate in the absence of the interaction between cloud and shortwave radiation. Therefore, the heat and moisture fluxes can be transported upward over the bay. A

higher relative humidity over the ocean induces the lower cloud base shown in Fig. 7.

In addition to the above mechanism, the local shortwave heating within the cloud may also have some contributions to the differences between the two cases. In the absence of shortwave heating, the cold cloud temperature (Fig. 9b) can lower the saturation water vapor pressure and enhance condensation, leading to the total water path increase in the NOSW run.

b. Longwave effects on cloud

Figure 12 shows the total water path for 1800 UTC of the NOLW simulation and should be compared with Fig. 3b. The removal of the longwave radiative interaction with condensate substantially decreases the total water path over the entire domain. In the CNTL run, the total water path within the land area is larger than 0.05 mm. For NOLW, this value is generally below 0.05 mm and the stratus cloud over the bay and some parts of the land disappeared. This emphasizes the importance of longwave radiation on cloud maintenance and development.

To understand why longwave radiation decreases the total water path, the vertically averaged turbulent kinetic energy for the CNTL and NOLW runs (see Fig. 10a and Fig. 13) were compared. The difference is small and could not account for the large difference in total water path.

The longwave radiative cooling rate for the CNTL simulation is displayed in Fig. 8b. It can be seen that longwave radiative cooling covers the entire cloud region. The maximum cooling rate is about 3.3 K h^{-1}. The cooling rate in the clear atmosphere is less than 0.5 K h^{-1}. It can be noted that the strong longwave cooling rates occurs at positions slightly higher than those for the strong shortwave heating rate (about a 50-m difference). Because of the cloud's greenhouse effect, a thin layer with a weak heating rate (less than 0.2 K h^{-1}) is located just below the cloud base. A comparison between Fig. 8a and Fig. 8b shows the longwave cooling rate dominates the shortwave heating rate throughout the entire cloud. The maximum heating rate (2.3 K h^{-1}) is approximately 30% less in magnitude than the maximum cooling rate (3.3 K h^{-1}). As a result, a colder cloud temperature relative to the environment formed (Fig. 9a). Thus, the effect of the net radiative cooling on the local condensation should be positive (i.e., the net radiative cooling can lower the saturation water vapor pressure, leading to enhanced condensation).

The elimination of longwave radiation effects does not make a large temperature change for the low-level atmosphere below the cloud (Fig. 9c). However, the cooler cloud temperature relative to the environment in the CNTL run disappears. The warmer cloud temperature in the NOLW run could produce local subsaturation and evaporation, which serves to decrease the total water path. Thus, the mechanism of radiation–condensation (evaporation) feedback pointed out by Sommeria (1976), Heymsfield and Miloshevich (1991), and Guan et al. (1997) is further supported by the current work.

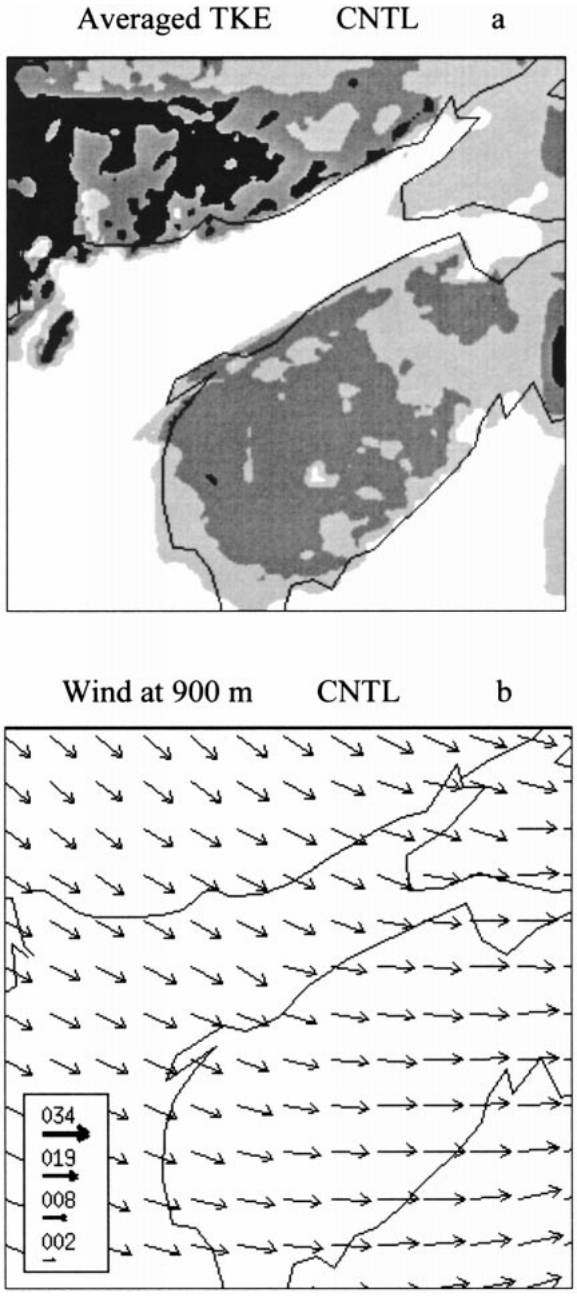

FIG. 10. (a) Vertical averaged turbulent kinetic energy at 1800 UTC 1 Sep 1995 for the CNTL run. The stippled areas from light to dark represent 0.1, 0.5, 1.0 m^2 s^{-2}, respectively. (b) Wind (knots) at 900 m at 1800 UTC 1 Sep 1995 for the CNTL run.

6. Summary and conclusions

In this paper, MC2 has been used to simulate and study an observed stratus cloud system over the Bay of

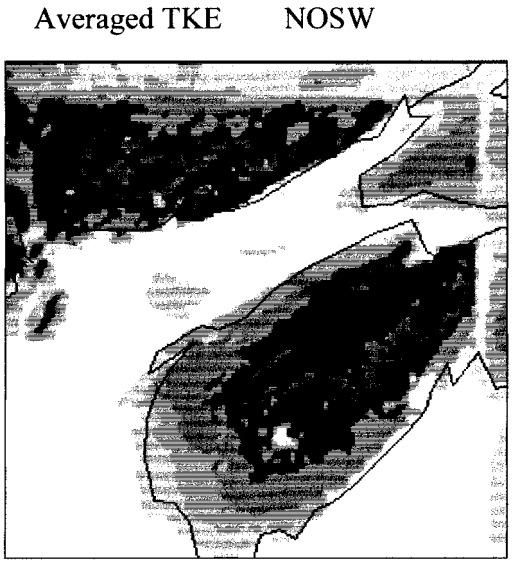

FIG. 11. Same as Fig. 10a but for the NOSW run. The stippled areas from light to dark represent 0.1, 0.5, 1.0, 1.5, 2.0 m^2 s^{-2}, respectively.

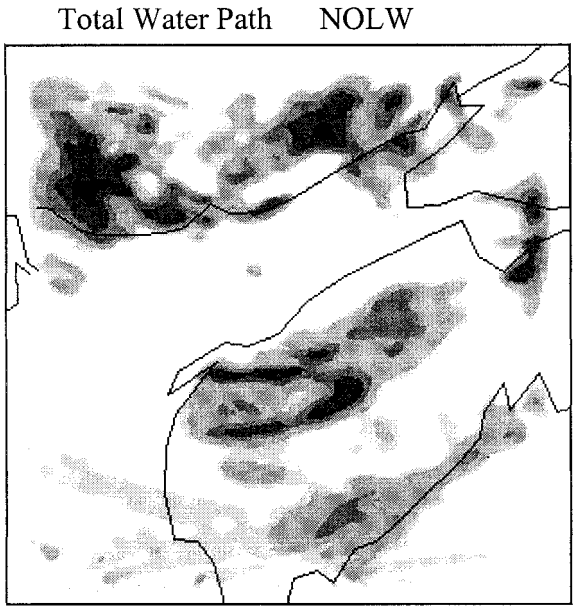

FIG. 12. Same as Fig. 3b but for the NOLW run.

Fundy during RACE. The model includes a new microphysics scheme (Tremblay et al. 1996). The longwave emissivity of the cloud and its visible optical depth were calculated in terms of the cloud water and ice water from the microphysics scheme. The relationship between cloud and radiation was fully interactive.

Observations from satellite, lidar, and aircraft were used to validate simulated cloud parameters and their radiative properties. To compare model predictions and airborne measurements, the selected model outputs were interpolated in space along the research aircraft trajectory. These series were then compared with aircraft measurements.

Some features of the stratus cloud systems were replicated in the high-resolution simulations. In particular, the cloud structure, position, liquid water content, temperature, and qualitative properties of the longwave and shortwave radiative fluxes were verified against the satellite, lidar, and aircraft observations. The observed clear region over the bay was also successfully predicted. The simulated cloud thickness (150 m) was thinner than the observed one (200–250 m). This could result from deficiencies in the cloud and radiation schemes. Another possible reason for the discrepancy is inaccuracies on the large-scale temperature, moisture, wind, and other fields forced on the nested domain. The vertical resolution also can be a factor, because $\Delta z = 50$ m is hardly adequate to resolve the fine vertical distribution of a 200 m deep cloud.

There are some quantitative differences between the simulated and observed radiative fluxes. The simulated downward shortwave radiative flux was significantly higher than observed within and below the cloud, while the simulated upward shortwave radiative flux was lower above the cloud top. It is clear that these differences are mainly induced by errors in the prediction of cloud thickness and cloud-top height. The disagreement in the droplet number concentration between the model and observations may also contribute to the differences in the shortwave radiative fluxes. For most of the flight, the observed and simulated downward longwave radiative fluxes are in fair agreement. A large difference was found only between the simulated and observed cloud top. The simulated upward longwave radiative flux is higher than observed, with an averaged difference

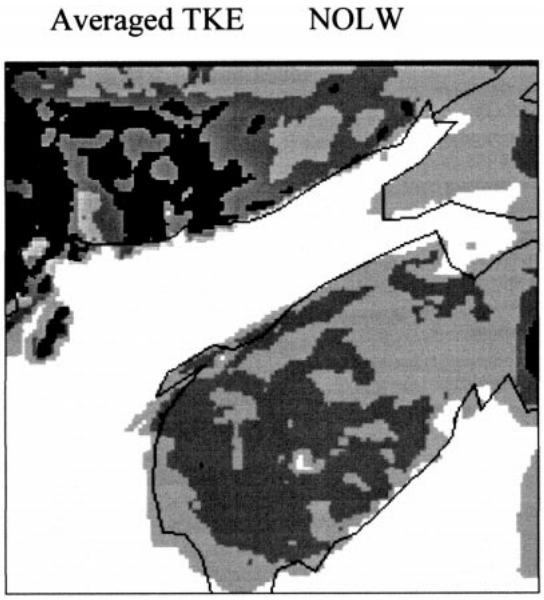

FIG. 13. Same as Fig. 10a but for the NOLW run.

of 30 W m^{-2}, which resulted from the use of a blackbody emissivity over the ocean and error in the sea surface temperature. A more reasonable value (0.94) should be used in the current Canadian forecast and MC2 models.

Two more numerical simulations (NOSW and NOLW runs) were designed to examine the effects of shortwave and longwave radiation on the simulated stratus cloud. The possible mechanisms responsible for those effects were also further explored.

Removing the shortwave radiative interaction with the cloud resulted in a substantial increase (approximately 3–6 times) in total water path. The cloud was cooler and the atmosphere below the cloud was warmer. Consequently, a more unstable low-level atmosphere was produced. The average difference in the lapse rate between the CNTL and NOSW runs within the selected cross-section was 1 K km^{-1}. In the meantime, an increase of turbulent kinetic energy within the low-level atmosphere was noted. This increase led to more upward transport of heat and moisture, and thus, more condensation. The local effect of shortwave heating on condensation may be also an important factor in the change of total water path.

When cloud absorption and emission of longwave radiation were turned off, the total water path within the entire domain exhibited significant decreases. The stratus cloud simulated in the CNTL and observed during RACE over the Bay of Fundy disappeared. In the absence of longwave cooling, the region corresponding to the cloud layer in the CNTL run was warmer, while the atmosphere below the CNTL cloud does not display a large change. The vertically averaged turbulent kinetic energy was very similar for both CNTL and NOLW runs. The difference in total water path is mainly due to the local effect of longwave radiation on condensation.

Acknowledgments. The authors would like to acknowledge Patrick King for the satellite image and Mark D. Couture for help in gathering and processing the aircraft data. The scientific and technical staffs of MSC and the National Research Council of Canada who helped obtaining the aircraft observations are gratefully acknowledged.

REFERENCES

Albrecht, B. A., 1993: Effects of precipitation on the thermodynamic structure of the trade wind boundary layer. *J. Geophys. Res.,* **98,** 7327–7337.

——, D. A. Randall, and S. Nicholls, 1988: Observations of Marine stratocumulus clouds during FIRE. *Bull. Amer. Meteor. Soc.,* **69,** 618–626.

——, C. S. Bretherton, D. Johnson, W. H. Schubert, and A. S. Frisch, 1995: The Atlantic Stratocumulus Transition Experiment—ASTEX. *Bull. Amer. Meteor. Soc.,* **76,** 889–904.

Barker, H. W., 1992: Solar radiative transfer through clouds possessing isotropic variable extinction coefficient. *Quart. J. Roy. Meteor. Soc.,* **118,** 1145–1162.

Bergeron, G., R. Laprise, and D. Caya, 1994: *Formulation of the Mesoscale Compressible Community (MC2) Model*. Cooperative Center for Research in Mesometeorology, 165 pp.

Boers, B., J. B. Jensen, P. B. Krummel, and H. Gerber, 1996: Microphysical and shortwave radiative structure of wintertime stratocumulus clouds over the Southern Ocean. *Quart. J. Roy. Meteor. Soc.,* **122,** 1307–1339.

Cahalan, R. F., W. Ridgway, W. J. Wiscombe, and T. L. Bell, 1994: The albedo of fractal stratocumulus clouds. *J. Atmos. Sci.,* **51,** 2434–2455.

——, D. Silberstein, and J. B. Snider, 1995: Liquid water path and plane–parallel albedo bias during ASTEX. *J. Atmos. Sci.,* **52,** 3002–3012.

Chen, C., and W. R. Cotton, 1983: A one-dimensional simulation of the stratus-capped mixed layer. *Bound.-Layer Meteor.,* **25,** 289–321.

Considine, G., J. A. Curry, and B. Wielicki, 1997: Modeling cloud fraction and horizontal variability in marine boundary layer clouds. *J. Geophy. Res.,* **102,** 13 517–13 525.

Desgagne, M., R. Benoit, and Y. Chartier, 1995: The Mesoscale Compressible Community Model (MC2) user's manual. Numerical Prediction Research Division, Atmospheric Environment Service, 51 pp.

Driedonks, A. G. M., and P. G. Duynkerke, 1989: Current problems in the stratocumulus-topped atmospheric boundary layer. *Bound.-Layer Meteor.,* **46,** 275–303.

Duynkerke, P. G., 1989: The diurnal variation of a marine stratocumulus cloud: A model sensitivity study. *Mon. Wea. Rev.,* **117,** 1710–1725.

Feingold, G., R. Boers, B. Stevens, and W. R. Cotton, 1997: A modeling study of the effect of drizzle on cloud optical depth and susceptibility. *J. Geophy. Res.,* **102,** 13 527–13 534.

Fouquart, Y., and B. Bonnel, 1980: Computations of solar heating of the earth's atmosphere: A new parameterization. *Contrib. Atmos. Phys.,* **53,** 35–62.

Fritsch, J. M., and C. F. Chappel, 1980: Numerical prediction of convectively driven mesoscale pressure systems. Part I: Convective parameterization. *J. Atmos. Sci.,* **37,** 1722–1733.

Garand, L., 1983. Some improvements and complements to the infrared emissivity algorithm including a parameterization of the absorption in the continuum region. *J. Atmos. Sci.,* **40,** 230–244.

——, and J. Mailhot, 1990: The influence of infrared radiation on numerical weather forecasts. *Proc. Seventh Conference on Atmospheric Radiation,* San Francisco, CA, Amer. Meteor. Soc., J146–J151.

Guan, H., M. K. Yau, and R. Davies, 1997: The effects of longwave radiation in a small cumulus cloud. *J. Atmos. Sci.,* **54,** 2201–2214.

Heymsfield, A. J., 1993: Microphysical structures of stratiform and cirrus clouds. *Aerosol-Cloud-Climate Interactions,* P. V. Hobbs, Ed., Academic Press, 97–121.

——, and L. M. Miloshevich, 1991: On radiation and latent heat feedback in clouds: Implications and a parameterization. *J. Atmos. Sci.,* **48,** 493–495.

Kogan, Y. L., M. P. Khairoutdinov, D. K. Lilly, Z. N. Kogan, and Q. Liu, 1995: Modeling of stratocumulus cloud layers in a large eddy simulation model with explicit microphysics. *J. Atmos. Sci.,* **52,** 2923–2940.

Kong, F.-Y., and M. K. Yau, 1997: An explicit approach of microphysics in MC2. *Atmos.–Ocean,* **35,** 257–291.

Koracin, D., and D. P. Rogers, 1990: Numerical simulations of the response of the marine atmosphere to ocean forcing. *J. Atmos. Sci.,* **47,** 592–611.

Krueger, S. K., G. T. McLean, and Q. Fu, 1995a: Numerical simulation of the stratus-to-cumulus transition in the subtropical marine boundary layer. Part I: Boundary layer structure. *J. Atmos. Sci.,* **52,** 2839–2850.

——, ——, and ——, 1995b: Numerical simulation of the stratus-to-cumulus transition in the subtropical marine boundary layer. Part II: Boundary-layer circulation. *J. Atmos. Sci.,* **52,** 2851–2868.

Kuo, H. L., 1974: Further studies on the parameterization of the influence of cumulus convection on large-scale flow. *J. Atmos. Sci.,* **31,** 1232–1240.

Moeng, C.-H., 1986: Large eddy simulation of a stratus-topped boundary layer. Part I: Structure and budgets. *J. Atmos. Sci.,* **43,** 2886–2900.

——, and U. Schumann, 1991: Composite structure of plumes in stratus-topped boundary layers. *J. Atmos. Sci.,* **48,** 2280–2291.

——, S.-H. Shen, and D. A. Randall, 1992: Physical processes within the nocturnal stratus-topped boundary layer. *J. Atmos. Sci.,* **49,** 2384–2401.

Nicholls, S., 1984: The dynamics of stratocumulus: Aircraft observations and comparisons with a mixed layer model. *Quart. J. Roy. Meteor. Soc.,* **110,** 783–820.

Robert, A., 1993: Bubble convection experiments with a semi-implicit formulation of the Euler equations. *J. Atmos. Sci.,* **50,** 1865–1873.

Rogers, D. P., and D. Koracin, 1992: Radiative transfer and turbulence in the cloud-topped marine atmospheric boundary layer. *J. Atmos. Sci.,* **49,** 1473–1486.

Rothman, L. S., and Coauthors, 1987: The HITRAN database: 1986 edition. *Appl. Opt.,* **26,** 4058–4097.

Slingo, J. M., 1989: A GCM parameterization for the shortwave radiative properties of water cloud. *J. Atmos. Sci.,* **46,** 1419–1427.

Sommeria, G., 1976: Three-dimensional simulation of turbulent processes in an undisturbed trade wind boundary layer. *J. Atmos. Sci.,* **33,** 216–241.

Strawbridge, K. B., and S.-M. Li, 1997: Optical properties of aerosols obtained from airborne lidar and several in-situ instruments during RACE. *Lidar Atmospheric Monitoring, Proc. EOS/SPIE,* Bellingham, WA, Society of Photo-Optical Instrumentation Engineers, 204–211.

Sundqvist, H., E. Berge, and J. E. Kristjansson, 1989: Condensation and cloud parameterization studies with a mesoscale numerical weather prediction model. *Mon. Wea. Rev.,* **117,** 1641–1657.

Szeto, K. K., A. Tremblay, H. Guan, D. R. Hudak, R. E. Stewart, and Z. Cao, 1999: The mesoscale dynamics of freezing rain storms over eastern Canada. *J. Atmos. Sci.,* **56,** 1261–1281.

Tanguay, M. A., A. Robert, and R. Laprise, 1990: A semi-implicit semi-Lagrangian fully compressible regional forecast model. *Mon. Wea. Rev.,* **118,** 1970–1980.

Tremblay, A., 1994: Simulations of the 15 July 1987 squall line using a fully compressible model. *Atmos.–Ocean,* **32,** 567–603.

——, A. Glazer, W. Yu, and R. Benoit, 1996: A mixed-phase cloud scheme based on a single prognostic equation. *Tellus,* **48A,** 483–500.

Yu, W., L. Garand, and A. P. Dastoor, 1997: Evaluation of model clouds and radiation at 100 km scale using GOES data. *Tellus,* **49A,** 246–262.

Zhang, D.-L., and J. M. Fritsch, 1986: Numerical simulation of the meso-β scale structure and evolution of the 1977 Johnstown flood. Part I: Model description and verification. *J. Atmos. Sci.,* **43,** 1913–1943.